https://arabjchem.org

Arabian Journal of Chemistry

Article in Press

Original article

Phosphate-responsive nanocomposite hydrogel laden with umbilical cord blood exosomes and nanosilver accelerates diabetic and infectious wound healing

Qianying Su[a], Peng Tuo[a], Huajian Li[a], Hanyi Mei[a], Yahong Yuan[a], Abid Naeem[b,*], Xiaoli Wang[a,*]

[a] *Hubei Key Laboratory of Embryonic Stem Cell Research, Hubei Clinical Research Center for Umbilical Cord Blood Hematopoietic Stem Cells, Taihe Hospital, Hubei University of Medicine, 442000 Shiyan, China.*

[b] *School of Life Science, Advanced Research Institute of Multidisciplinary Science, School of Medical Technology, Key Laboratory of Molecular Medicine and Biotherapy, Key Laboratory of Medical Molecule Science and Pharmaceutics Engineering, Beijing Institute of Technology, 100081 Beijing, China.*

ARTICLE INFO

Keywords:
Antimicrobial activities
Diabetic wound healing
Exosomes
Hydrogel
Nanosilver

ABSTRACT

Chronic non-healing wounds are a significant global health challenge, particularly for individuals with diabetes, requiring advanced therapeutic strategies. This study focuses on the development and assessment of phosphate-responsive hydrogel designed for the release of nanosilver and umbilical cord blood exosomes (UCB-exos), to promote wound closure in diabetics, as well as tissue regeneration. The findings indicate that UCB-exos effectively promotes skin fibroblast proliferation and migration and maintains endothelial angiogenic activity in hyperglycemic conditions. By modulating the cell cycle signaling pathway, UCB-exos improve the biological functions of endothelial cells in a hyperglycemic environment. Exosomes were incorporated into a nanosilver hydrogel to evaluate their potential for promoting diabetic wound healing *in vivo*. The hydrogel not only promoted collagen deposition and angiogenesis but also demonstrated significant antimicrobial activity, thereby expediting the wound healing process. This study illustrates that the phosphate-responsive nanocomposite hydrogel, incorporating UCB-exos and nanosilver, effectively enhances the healing of diabetic and infectious wounds. It has therapeutic potential in treating diabetic wounds and highlights the promising application of such composite hydrogels for managing chronic, non-healing diabetic wounds.

1. Introduction

Improvements in quality of life and an aging population have contributed to the increasing prevalence of diabetes mellitus and chronic ulcers, such as diabetic wounds, making their management more challenging [1]. Diabetic wounds often demonstrate impaired healing due to elevated blood glucose levels, which facilitate bacterial proliferation and consequently extend the wound healing process [2]. Currently, modern medical practices focus on reducing local pressure, preventing infection, and promoting revascularization in conjunction with blood glucose management to address diabetic wound healing [3]. However, the efficacy of these approaches is often suboptimal. Consequently, the exploration of novel treatment strategies for diabetic wound healing holds significant importance in enhancing the prognosis of diabetic foot ulcers, mitigating the need for amputation, enhancing patient quality of life, and reducing healthcare expenditures.

Recent scientific developments have shown that a significant focus has been directed toward the utilization of stem cell-derived exosomes for the enhancement of diabetic wound healing [4]. Exosomes, characterized by their extracellular vesicular nature and size ranging from 30 to 200 nm, play a crucial role as mediators of cellular paracrine signaling and are extensively employed in the realms of tissue regeneration and repair [5]. These exosomes, originating from stem cells, can be regarded as paracrine mediators that significantly contribute to the regulation of inflammation, promotion of angiogenesis, stimulation of epithelial neogenesis, and facilitation of collagen deposition in wound healing [6]. Despite their promising ability to accelerate skin wound recovery, exosomes are susceptible to rapid immune system clearance and possess a limited half-life, thereby constraining their therapeutic effectiveness. Wound dressings with high efficacy serve as a barrier to facilitate prompt wound closure and reduce scar formation. Since hydrogels are both biodegradable and biocompatible, they are widely utilized in tissue repair and wound healing applications [7]. It functions not only as a scaffold for cell support in tissue regeneration but also as an efficient vehicle for drug delivery. Numerous studies have shown that the simultaneous application of various types of exosomes and hydrogels in wound healing not only protects the exosomes from premature degradation but also enables their sustained release, thereby producing a synergistic therapeutic effect [8-11]. Compared to direct exosome injection, exosome-loaded hydrogels offer the potential to significantly increase the retention time and stability of exosomes, thereby reducing the need for repeated administrations and enhancing therapeutic efficacy. This study utilized exosomes derived from umbilical cord blood (UCB), which are characterized by low immunogenicity, high biocompatibility, ease of access and storage, versatility, and high yield. These attributes render them particularly promising for applications in wound healing treatment.

Wounds associated with diabetes present a significantly elevated risk of bacterial infection within high-glucose environments, thereby impeding their healing process [12]. Inorganic nanoparticles with small

*Corresponding authors.
E-mail addresses: anaeemktk@gmail.com (A. Naeem), xiaolitina@126.com (X. Wang).

Received: 21 October 2024 **Accepted:** 07 December 2024 **Epub Ahead of Print:** 11 March 2025 **Published:** ***

DOI: 10.25259/AJC_103_2024

size (5–200 nm) and high specific surface area can penetrate bacterial biofilm and kill drug-resistant bacteria for antibacterial infection [13]. In wound healing, different metal nanoparticles have been reported to have antimicrobial properties, such as silver, gold, zinc, copper, and titanium [14-18]. The antimicrobial efficacy of silver nanoparticles (Ag NPs) is primarily attributed to their ability to release Ag^{+} ions upon dissolution. It is these ions that interact with the phosphorus- and sulfur-containing protein groups located in the bacterial cell wall and plasma membrane, resulting in the disruption of the cell membrane and subsequent leakage of cytoplasmic contents. This process ultimately culminates in bacterial cell death [19]. Although inorganic nanoparticles have excellent antimicrobial properties, the disadvantages of high toxicity, weak molecular recognition, poor controllability, short drug validity, and susceptibility to rapid clearance limit their clinical use. Consequently, by combining biocompatible polymer materials with inorganic nanoparticles, nanocomposite hydrogels with diverse structures can be produced to significantly reduce the toxic effects of inorganic nanomaterials on human bodies, as well as to achieve local and long-lasting drug release, which will allow drugs to perform their antimicrobial effects more effectively [20].

This study developed a composite hydrogel integrating biocompatible polymers, inorganic nanoparticles, and umbilical cord blood exosomes (UCB-exos). Initially, a self-assembly process was employed to combine polyacrylic acid (PAA) with Ca^{2+}, forming the fundamental biomimetic mineralized hydrogels. UCB-exos and AgNPs were then incorporated into the hydrogel, resulting in the formation of the composite hydrogel name as PAA-CaP@ AgNps@exo hydrogel (Scheme 1a). Then, a model of diabetic rats with full-thickness skin defects or infected wounds was established to evaluate the effects of this hydrogel on the wound healing process (Scheme 1b,c). The PAA-CaP@AgNps@exo hydrogel, characterized by its exosome-releasing and antibacterial properties, effectively aids diabetic skin wound regeneration. It shows therapeutic promise for treating chronic, non-healing diabetic wounds, highlighting the potential of composite hydrogels in wound management.

2. Materials and Methods

2.1. Separation and identification of exosomes

UCB samples were collected from healthy neonates following the acquisition of informed consent from the mothers and approval from the Hubei University of Medicine Ethics Committee (2024KS49). As a first step, the plasma was separated from the UCB samples by centrifugation at 300×g for 10 mins at 4°C. Then, the plasma underwent sequential centrifugation at 300×g for 10 mins, 2000×g for 10 mins, and 8000×g for 35 mins, all conducted at 4°C. Subsequently, the resultant supernatant was further centrifuged at 100,000×g for 70 mins at 4°C to ensure complete removal of the liquid phase. The resulting precipitate was resuspended in phosphate-buffered saline (PBS). The protein concentration of the exosome was quantified by a bicinchoninic acid (BCA) assay kit (Beyotime, China). The UCB-exos were either utilized for experimental procedures or stored at -80°C for future use.

Transmission electron microscopy (TEM) was used to investigate the morphology of the exosome, while its size was determined with a Zeta sizer (ZS90). Surface markers of the exosome were identified using Western blot analysis. Sodium dodecyl sulfate-polyacrylamide gel electrophoresis (SDS-PAGE) was used to isolate the exosome protein, then transferred to a polyvinylidene fluoride (PVDF) membrane. The membrane was incubated overnight with antibodies against CD9 (1:1000, Proteintech, USA), CD63 (1:1000, Proteintech), CD81 (1:1000, Proteintech), TSG101 (1:1000, Proteintech), and Glyceraldehyde-3-phosphate dehydrogenase (GAPDH) (1:1000, Proteintech). Following this, it was incubated with secondary antibodies for 1h. Chemiluminescence gel imaging (Bio-Rad) and enhanced chemiluminescence detection kits (Beyotime, China) were used to visualize and analyze protein bands.

2.2. Uptake of UCB-exos

To label exosomes, the PKH67 kit (Sigma) was employed as per the manufacturer's guidelines. The labeled exosomes were then

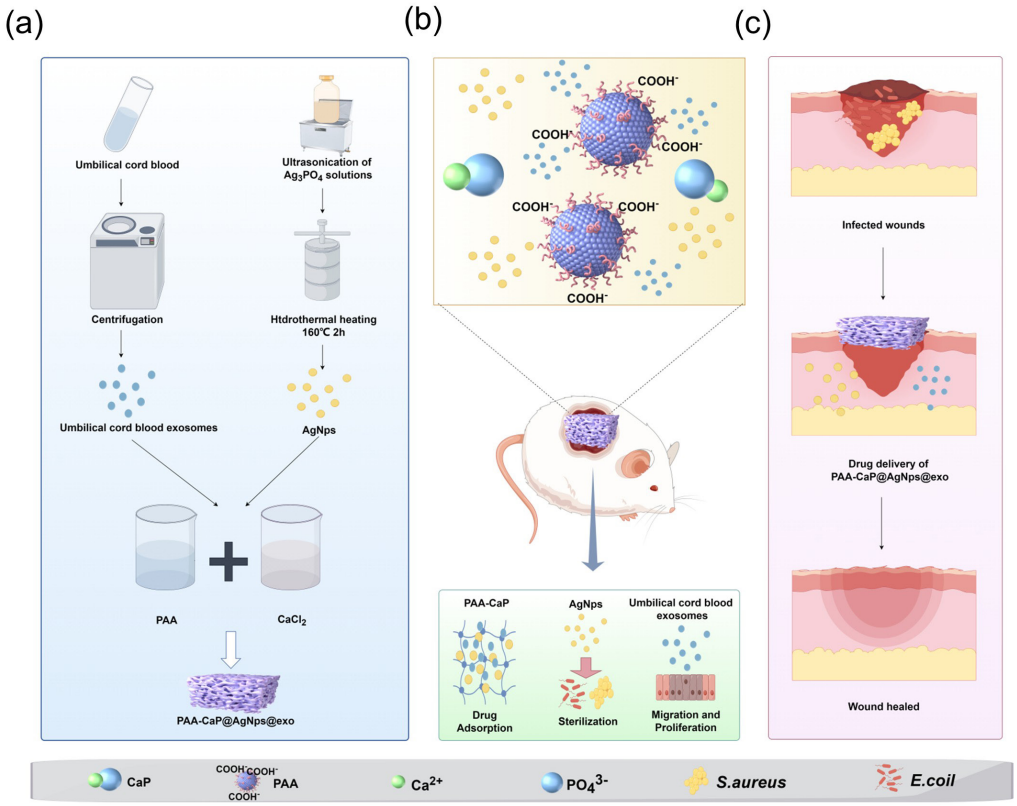

Scheme 1. Preparation and application of the PAA-CaP@AgNps@exo hydrogel for healing diabetic wounds (by Figdraw). (a) Construction of the PAA-CaP@AgNps@exo hydrogels; (b) PAA-CaP@AgNps@exo hydrogel application for healing diabetic wounds; and (c) PAA-CaP@AgNps@exo hydrogel application for healing infected diabetic wounds. CaP: calcium phosphate; PAA: polyacrylic acid

incubated with the cells at 37°C in a 5% CO_2 environment for 24 hrs. After incubation, the cells were fixed with 4% paraformaldehyde for 15 mins, then stained with 4',6-diamidino-2-phenylindole (DAPI) (Beyotime). Fluorescence signals were analyzed with a Leica DMI6000B microscope.

2.3. Cell proliferation, migration, and tube formation assays

Human umbilical vein endothelial cells (HUVEC) were procured from the China Center for Type Culture Collection (Wuhan, China). Minimum essential medium alpha (MEM-alpha) (Gibco) supplemented with 10% fetal bovine serum (FBS) (Gibco) and 1% penicillin-streptomycin solution (Beyotime) was used to culture these cells. Dulbecco's modified eagle medium (DMEM) (Gibco) supplemented with 10% FBS was used to culture human skin keratinocytes HaCaT (FuHeng Biology, Shanghai, China). The cells were incubated in the incubator at 37°C, 5% CO_2. The cells were divided into three groups: 1) Negative control (NC) group: culture medium; 2) High Glucose (HG) group: 30 mM Glucose; and 3) HG+exos group: 30 mM Glucose+UCB-exos for the cell proliferation, migration, and tube formation experiments.

2.3.1. Cell proliferation assay

The xCELLigence real-time cell analysis (RTCA) system (ACEA Biosciences Inc., USA) was used to measure the proliferation of cells. Overall, 5,000 cells were plated per well, and three replicate wells were assigned to each experimental group. Monitoring and recording of cell proliferation were conducted continuously at 15 mins intervals over a 96 hrs period. The cell index, automatically calculated by the RTCA software, served as a real-time metric for evaluating cell behavior.

2.3.2. Scratch wound healing assay

Both the scratch assay and transwell system methodologies were employed to determine cell migration. The wound-healing study was conducted in 6-well plates after the cells had reached full confluence. A linear scratch was formed in the cell monolayer with the help of a 10 μL pipette tip. The cell layer was then rinsed with PBS three times, then incubated for 24 hrs with serum-free medium in the incubator at 37°C and 5% CO_2. The width of the scratches was quantified to compare migration rates across various groups, and the mean width was computed at both 0 and 24 hrs.

2.3.3. Transwell migration assay

Transwell assays were conducted in triplicate utilizing a 24-well transwell plate (Corning). Briefly, 1×10^5 cells were suspended in 200 μL of DMEM in the upper chamber, and the lower chamber was added with 600 μL of DMEM supplemented with 10% FBS, either alone or in combination with exosomes. After 24 h, the cells adhering to the underside of the filter membrane were fixed and subsequently stained with crystal violet. The migration of cells was assessed by counting them in five randomly chosen fields under a microscope.

2.3.4. Tube formation assay

Briefly, about 25,000 HUVECs were seeded in 96-well plates coated with matrigel. Observation of tube formation was performed under a microscope following 6 hrs of incubation, and an angiogenesis plugin for ImageJ was used to measure the length of endothelial tubes.

2.4. RNA-sequencing

RNAs were extracted from HUVECs exposed to high glucose, with or without exosomes, and sequenced by Aksomics (Shanghai, China) using Illumina. The differential genes were then analyzed for biological process (BP), cell components (CC), molecular function (MF), and Kyoto Encyclopedia of Genes and Genomes (KEGG) pathways.

2.5. Analysis of the cell cycle by flow cytometry

HUVECs (1×10^6) from various treated groups were collected and stained by a cell cycle analysis kit (Beyotime) following the manufacturer's protocol, then the flow cytometry was conducted with a FACScan flow cytometer (BD Biosciences) and analysis using ModFit software.

2.6. Preparation of PAA-CaP@Ag Nps@exo hydrogels

First, Ag nanoparticles (AgNps) were synthesized by dissolving 90 mL of a 0.15 mol/L $AgNO_3$ solution in a 600 mL 4.5 mmol/L Na_2HPO_4 solution. The resulting precipitate was subsequently suspended in deionized water and subjected to hydrothermal heating at 160°C for a period of two hrs and dried into a powdered form. After that, 8 mg of AgNps were added into 4 mL of phosphate buffer and dispersed using an ultrasonicator to create solution A. Then, combined 10 mL of 7.22 mg/mL PAA, 10 mL of 0.1 mol/L $CaCl_2$ solution, and 60 μg UCB-exos at room temperature to form solution B. Finally, solution A was added to solution B at the rate of 1 mL/min and stirred at 500 rpm for 30 min until the mixture transitioned from clarified to turbid, resulting in the formation of the PAA-CaP@AgNps@exo hydrogels.

2.7. Characterization of PAA-CaP@Ag Nps@exo hydrogels

The morphology of the freeze-dried hydrogels was studied through scanning electron microscopy (SEM). A NanoSEM 200 electron microscope operating at a 10 kV acceleration voltage was used to observe the samples. A Fourier Transform Infrared Spectrometer (FTIR) (Nicolet iS50, Thermo-Fisher, USA) was used to determine the chemical composition of the hydrogels. A Nano-Zs Malvern nano analyzer was used to detect the particle size. The structural characterization of the hydrogels was conducted using X-ray diffraction (XRD) analysis with a RINT-2000 Rigaku diffractometer (Rigaku, Tokyo, Japan). The quantitative elemental analysis and spatial distribution of elements within the hydrogels were performed using energy-dispersive X-ray spectroscopy (EDX). Elemental data and EDX mapping analyses were conducted with a Zeiss Ultra Plus SEM (ZEISS, Germany).

2.8. The release kinetics of exosome from PAA-CaP@AgNPs@exo hydrogels

In vitro release kinetics of UCB-exo from the hydrogels were evaluated by slightly modifying the previously reported method [21]. Briefly, the PAA-CaP@exo and PAA-CaP@AgNPs@ exo nanoparticle hydrogels were incubated in sterile PBS at 37°C. The protein content of UCB-exos was quantified using the microBCA protein assay (System Biosciences) following the manufacturer's protocol.

2.9. The release kinetics of Ag^+ and Ca^{2+} from PAA-CaP@AgNPs@exo under phosphate response

Equal quantities of PAA-CaP@AgNps@exo dry hydrogels were immersed in PBS solutions with molarities of 0, 0.01, and 0.05 M. The solutions were subsequently extracted at 37°C at 0, 6, 12, 24, and 48 hrs. Following extraction, 10% nitric acid (HNO_3) was added to the solutions, and they were then filtered through a needle filter with 0.22 μm. Inductively coupled plasma optical emission spectrometry was used to detect the concentrations of Ag^+ and Ca^{2+}.

2.10. In vitro antimicrobial activity

The disc diffusion method was used to evaluate the antimicrobial efficacy of hydrogels against *Staphylococcus aureus* (*S. aureus*) and *Escherichia coli* (*E. coli*). The hydrogels were applied to agar plates inoculated with *S. aureus* and *E. coli* and then incubated at 37°C. After 24 hrs, the diameters of the inhibition zones were measured and recorded.

2.11. Diabetic wound and diabetic wound infection models

Sprague-Dawley (SD) rats (Male, 8 weeks old, 200-220 g) were housed in an environment maintained at constant temperature and humidity. A dose of 65 mg/kg of streptozotocin (STZ) was administered intraperitoneally to the rats. Two weeks post-injection, blood glucose levels were assessed using a blood glucose monitor. Rats exhibiting blood glucose concentrations exceeding 16.67 mmol/L were

classified as diabetic. To develop a diabetic wound model, diabetic rats were anesthetized *via* intraperitoneal administration of Nembutal at a dosage of 35 mg/kg (Sigma, USA). Following the induction of anesthesia, the dorsal skin of each rat was shaved and sterilized using 75% ethyl alcohol. Subsequently, a full thickness square wound measuring 1.5 cm on each side was surgically created on the dorsum of each mouse. Then, a total of 15 rats were randomly divided into 5 groups of three: Blank control group (BC); Aquacell ® wound dressing was used for a positive control group (PC); PAA-CaP@AgNps; PAA-CaP@exo group; and PAA-CaP@AgNps@exo group. A wound area measurement was performed using Image J on days 0, 4, 8, 12, and 16. The Hubei University of Medicine Animal Care and Use Committee approved this experiment (2024-55). The diabetic wound infection model was developed by anesthetizing diabetic rats and making wounds in the same manner as the diabetic wound model for rats. Then, *S. aureus* and *E. coli* bacteria were inoculated into the wounds at a 1:1 ratio. Three days after infection, six rats were randomly divided into two groups of three per group: PBS (control) group and PAA-CaP@Ag Nps@exo group. Digital photographs were captured on days 0, 4, 8, 12, and 16, and the wound area was quantified utilizing ImageJ software. This study received approval from the Hubei University Animal Care and Use Committee (approval number: 20240034). The rate of wound closure was calculated by assessing the wound area in each group through the delineation of wound boundaries with software (ImageJ). According to the following formula, wound closure rates (%) were calculated as follows: Wound closure rate (%) = [(S (0 day) - S (n day)/S (0 day)] × 100%, where S represents the wound area.

2.12. Histology, immunohistochemistry, and immunofluorescence analysis

A specimen of fully thickened traumatic tissue, measuring approximately 3 mm in size, was obtained from the peripheral margin of the entire wound and promptly fixed in a 4% paraformaldehyde solution. After 24 hrs, the skin wounds underwent dehydration overnight and were subsequently embedded in paraffin. Tissue sections were mounted on glass slides for histological examination. Hematoxylin and eosin (H&E) staining, along with Masson's trichrome staining, were conducted to visualize pathological alterations within the tissue. Furthermore, paraffin-embedded skin wound sections were sliced and subjected to immunohistochemical analysis for CD31 (Proteintech, 28083-1-AP, 1:4000), Ki67 (Proteintech, 28074-1-AP, 1:2000), CD206 (Proteintech, 18704-1-AP, 1:1000), CK10 (Proteintech, 16855-1-AP, 1:200), Collagen I (Proteintech, 67288-1-Ig, 1:3000), and Collagen III (Proteintech, 22734-1-AP, 1:1000). Photographs were taken using a microscope and digital camera. To assess the presence of pro-inflammatory cytokines at the wound site, immunofluorescence analysis was conducted on wound sections on the seventh day post-injury. We incubated the tissue sections with anti-IL-1 rabbit polyclonal antibody (pAb) (Servicebio, 1:500) and anti-tumor necrosis factor (TNF)-αrabbit pAb (Servicebio, 1:200), followed by incubation with a goat anti-rabbit IgG Alexa Fluor® 594-conjugated secondary antibody (Abcam, 1:500) and DAPI for nuclear staining. Stained sections were imaged using a fluorescent microscope, and the percentage of positively stained cells in each experimental group was calculated using Image-Pro Plus software.

2.13. Statistical analysis

Statistical analyses were conducted employing GraphPad Prism software. Data were expressed as mean ± standard deviation (SD). One-way analysis of variance (ANOVA) was used to determine statistically significant differences between groups, with p-values less than 0.05 regarded as significant.

3. Results and Discussion

3.1. Exosomes characterization

UCB-exos were isolated *via* ultracentrifugation. Different characterization techniques such as western blotting, nanoparticle tracking analysis (NTA), and TEM analysis were used to identify the harvested UCB-exos. The Western blotting analysis confirmed the presence of CD9, CD63, CD81, and TSG101 in the isolated UCB-exos compared with the peripheral blood mononuclear cells (PBMCs) (Figure 1a). NTA suggested that the size distribution of UCB-exos displayed a single peak at approximately 100 nm (Figure 1b). As shown by TEM, UCB-exos have a typical “saucer-like” structure (Figure 1c). Together, these results confirmed the extraction of UCB-exos had been successful. Exosomes labeled with PKH67 were co-cultured with HUVEC in order to further clarify whether UCB-exos are capable of being endocytosed into cells. Our observations indicate that PKH67-labeled exosomes, identifiable by their green fluorescence, were predominantly localized in the perinuclear region of human umbilical vein endothelial cells (HUVECs), as illustrated in Figure 1(d). This finding substantiates the internalization of exosomes by endothelial cells.

3.1.1. The influence of UCB-exos on keratinocytes and endothelial cells under high glucose conditions

Keratinocytes and endothelial cells play a vital role in wound healing [22]. To examine the effects of UCB-exos on keratinocytes and endothelial cells function under high glucose. HaCaT cells and HUVECs were treated with LG, HG, and HG+exos, respectively. The proliferation of HaCaT cells and HUVECs was detected by RTCA assay. We found that high glucose concentration inhibits the proliferation of cells. At the same time, UCB-exos promoted cell proliferation under high glucose conditions (Figure 2a). The UCB-exos treatment significantly enhanced cell migration under high glucose conditions compared to the HG group, as demonstrated by the scratch wound healing assay (Figure 2b) and the transwell migration assay (Figure 2c). Then, the impact of UCB-exos on the angiogenic activities of endothelial cells was assessed. The matrigel tube formation assay serves as an *in vitro* model for studying angiogenesis. As shown in Figure 2(d), HUVECs treated with UCB-exos produced more capillary-like structures in high glucose conditions compared with the HG group. These results demonstrate the potential of UCB-exos in protecting the biological functions of keratinocytes and HUVECs *in vitro* under high glucose conditions.

3.1.2. Mechanism of UCB-exos regulating the biological functions of endothelial cells

To elucidate the underlying mechanisms by which UCB-exos influence the biological functions of endothelial cells under hyperglycemic conditions, transcriptome sequencing on endothelial cells treated with UCB-exos in a high glucose environment was performed. The results were compared to those of a control group subjected solely to high glucose conditions, and the findings are presented in the accompanying heatmap (Figure 3a). A total of 934 significantly different genes were

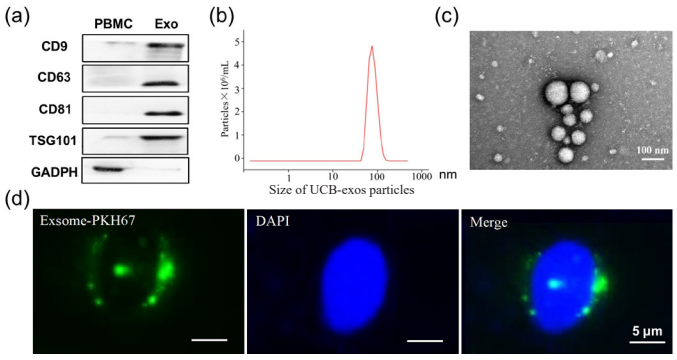

Figure 1. UCB exosome identification. (a) Exosome-specific markers such as Tetraspanin 9 (CD9), Lysosomal membrane-associated glycoprotein 3 (CD63), CD81, and Tumor susceptibility antigen 101 (TSG101) were detected by Western blot; (b) Nanoparticle tracking analysis (NTA) for determining the size of exosome particles (30 to 150 nm); (c) Morphological observation of exosomes under transmission electron microscopy; and (d) Internalization of PKH67-labelled exosomes by cells was observed using laser confocal microscopy. PBMCs: peripheral blood mononuclear, GAPDH: Glyceraldehyde-3-phosphate dehydrogenase, Exo: exosomes, DAPI: 4’,6’-Diamidino-2-phenylindole, Blue is the nucleus, Green is the exosomes.

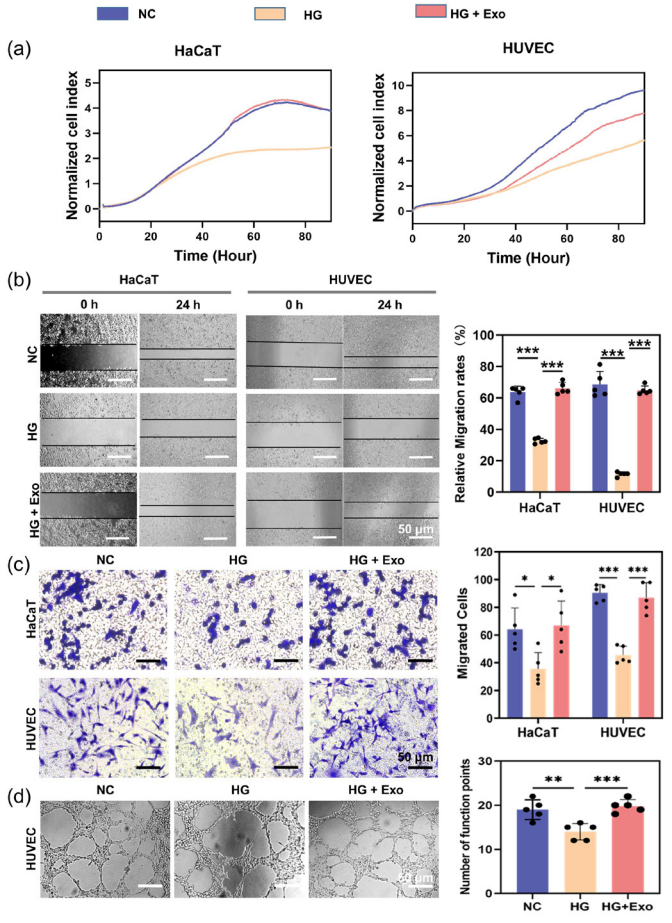

Figure 2. The influence of umbilical cord blood exosomes (UCB-exos) on keratinocytes and endothelial cells under high glucose conditions. (a) Detection of the proliferation of human skin keratinocytes (HaCaT) cells and Human umbilical vein endothelial cells (HUVEC) with UCB-exos by real-time cell analysis (RTCA) assay; (b) Determination of the cell migration (the Migrated cells were stained purple by crystal violet.) of HaCaT cells and HUVECs with UCB-exos by scratch wound healing assay; (c) Detection of the cell migration of HaCaT cells and HUVECs with UCB-exos by transwell assay; (d) Assessment of the impact of UCB-exos on angiogenic activities of HUVECs by tube formation assay (n = 3, mean ± SD, *p < 0.05, **p < 0.01, ***p < 0.001). The black dots represent the experimental results from independent repetitions of the experiment. The Migrated cells were stained purple by crystal violet. HG: High glucose, NC: Negative control.

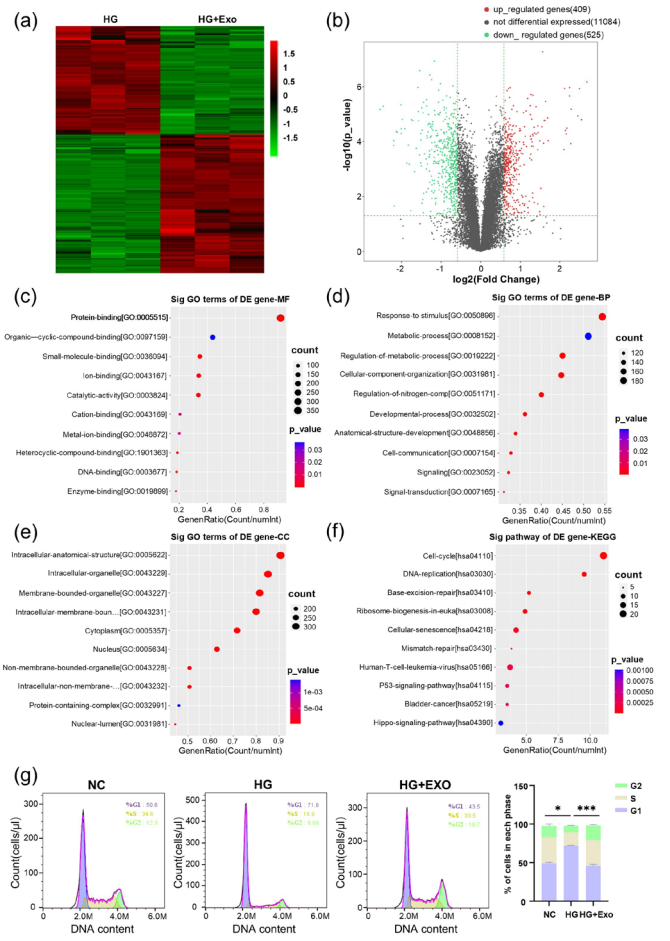

Figure 3. The underlying mechanism of the effect of umbilical cord blood exosomes (UCB-exos) on the biological functions of endothelial cells under high glucose. (a) The heatmap of Human umbilical vein endothelial cells (HUVECs) and HUVECs treated with UCB-exos under high glucose by transcriptome sequencing; (b) The volcanic map of HUVECs and HUVECs treated with UCB-exos under high glucose by transcriptome sequencing; (c-e) Gene Ontology (GO) function enrichment analysis molecular function (MF), biological process (BP), and cell components (CC); (f) Transcriptome sequencing enrichment results of the Kyoto encyclopedia of genes and genomes (KEGG) pathway; (g) Analysis of cell cycle stages of HUVECs, and HUVECs treated with UCB-exos under high glucose by flow cytometry (n = 3, mean ± SD, *p < 0.05, **p < 0.01, ***p < 0.001). The pink peak represent G1 phase of the cell cycle and the blue peak represent G2 phase of the cell cycle. HG: High glucose, NC: Negative control

obtained, including 409 differentially up-regulated genes and 525 differentially downregulated genes. The distribution of differential genes was generated to show in the volcanic map (Figure 3b). Moreover, GO function enrichment analyses were also carried out. The results are shown in Figures 3(c-e). According to the enrichment results of GO's molecular function, biological process, and cell components, these genes are associated with biological processes such as the regulation of protein binding, response to stimulus, and intracellular anatomical structure. The enrichment results of the KEGG pathway showed that it mainly regulated the cell cycle signaling pathway (Figure 3f). Flow cytometry was used to determine the distribution of cells during the G1, S, and G2 phases of the cell cycle. The result showed that the cell cycle was halted at the transition from G1 to S-phase under glucose conditions, and this was reversed by being treated with UCB-exos (Figure 3g). It shows that UCB-exos have the potential to influence the bioactivity of endothelial cells in hyperglycemic conditions *via* multiple mechanisms.

3.2. Nanocomposites hydrogels characterization

To characterize the morphological structure of AgNPs, the spherical silver nanoparticles coated with phosphate were determined through TEM analysis, whereas the average particle diameter was determined through dynamic light scattering (DLS), which showed a diameter of approximately 40.2±13.6 nm (Figure 4a,b). SEM was used to investigate the hydrogel's internal structure. The hydrogel shows an interconnected porous network structure, and the distribution of AgNps and UCB-exos into hydrogel is shown to be quite constant and homogeneous (Figure 4c). The composition and elemental constituents of the hydrogel were further examined utilizing EDS. The findings, presented in Figure 4(d-f), demonstrate that Ag nanoparticles were successfully incorporated into the hydrogel through the biomimetic mineralization technique. The XRD measurements were performed to examine the phase analysis of AgNps and PAA-CaP@AgNps (Figure 4g). According to the results, the characteristic peaks of AgNps disappeared after embedding in the PAA-CaP hydrogel, which also indicated that the AgNps had been immobilized in the PAA-CaP hydrogel. To assess and check the formation of cross-linked hydrogel networks with AgNPs and UCB-exos, the samples were analyzed by FTIR. In the FTIR spectra shown in Figure 4(h), the presence of characteristic peaks of hydrogen phosphate at 1130 cm^{-1} and 987 cm^{-1}, shows the successful loading of AgNps. The absorption peaks near 1700 cm^{-1} were obviously enhanced, indicating the successful loading of the exosome, and the change of the COO^- characteristic peaks near 1554 cm^{-1} and 1454 cm^{-1} speculated that the exosome had an effect on

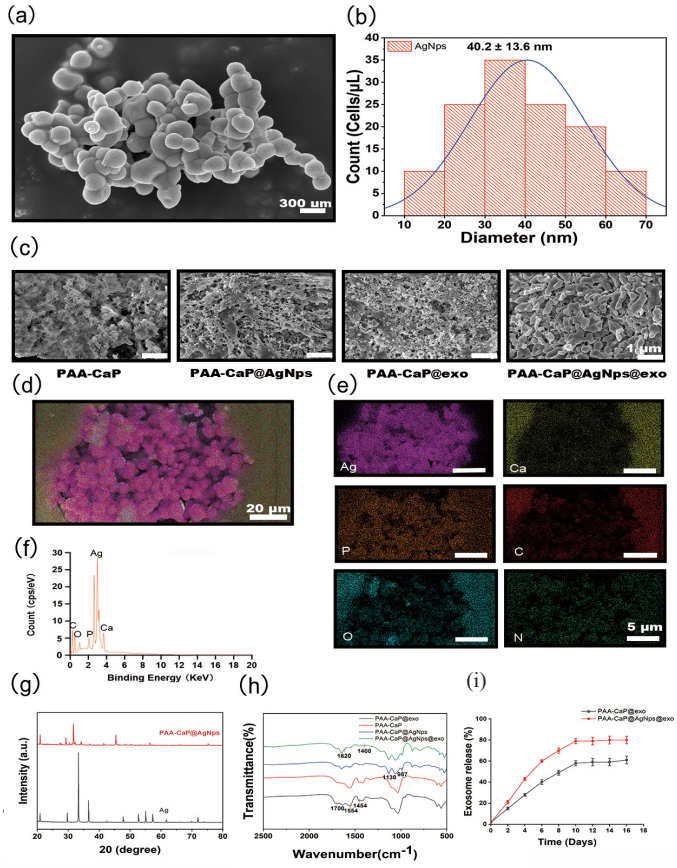

Figure 4. Characterization of the nanocomposites hydrogels. (a) Scanning electron microscopy (SEM) analysis of the morphological structure of AgNPs; (b) Determination of the size of AgNPs by dynamic light scattering (DLS) measurement; (c) SEM analysis for the morphological structure of PAA-Cap, PAA-Cap@AgNps, PAA-Cap@exo, and PAA-CaP@AgNps@exo hydrogels; (d-f) Analysis of the composition and elemental constituents of PAA-CaP@AgNps@exo hydrogel by energy dispersive spectrometer (EDS); (g) Analysis of the phase of AgNps and PAA-CaP@AgNps by X-ray diffraction (XRD) measurements; (h) PAA-Cap@ AgNps@exo hydrogel was analyzed by Fourier transform infrared spectrometer (FTIR); (i) Detecting exosome release from PAA-Cap@AgNps@exo hydrogels in phosphate buffered saline (PBS) solution by micro Bicinchonic acid assay (BCA) protein assay.

the COO^- coordination. Comparing PAA-CaP@AgNps with PAA-CaP@AgNps@exo, it can be found that the carboxylate characteristic peaks near 1620 cm^{-1} and 1400 cm^{-1} were significantly weakened, suggesting that the exosome was successfully loaded to PAA-CaP@AgNps. To assess the release of the exosomes from the exosome-loaded hydrogel, the hydrogel was immersed in PBS solution. Based on the MicroBCA protein assay, gradual exosome release was observed over a period of 16 days from the hydrogel (Figure 4i). These results confirmed that the exosomes could gradually be released from the hydrogel and exosomes were successfully loaded into the hydrogel.

3.2.1. Phosphate response degradation of the PAA-CaP@AgNps@exo hydrogel

Due to the precipitation/dissolution equilibrium of CaPs in phosphate buffer solution, the dissolution of CaPs as cross-linking points may lead to degradation of PAA-CaPs@AgNps@exo hydrogel. To investigate the effect of different phosphate concentrations on hydrogel degradation, Ca^{2+}, and Ag^+ release from the hydrogels by treating them with different concentrations of PBS at different times were detected, respectively (Figure 5a). The findings indicated that elevated phosphate concentrations could diminish Ca^{2+} release, with Ca^{2+} release initially increasing during the first six hours and stabilizing after twelve hours (Figure 5b). In contrast, Ag^+ exhibited an inverse response to phosphate concentration, as the high levels of PO_4^{3-} in PBS interacted with Ag^+ to form a precipitate (Ag_3PO_4), thereby enhancing Ag^+ release. The release

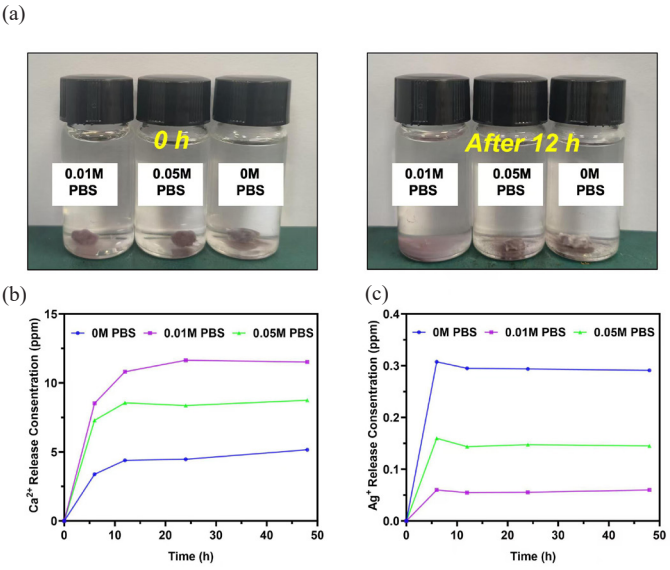

Figure 5. Phosphate response release Ca^{2+} and Ag^+ from the PAA-CaP@AgNps@exo hydergel. (a) Degradation of the hydrogel with different concentrations of phosphate buffered saline (PBS) for different times; (b) Determination of the release of Ca^{2+} from the hydrogels by treating with different concentrations of PBS for different periods of time by Inductively coupled plasma optical emission spectroscopy (ICP-OES); (c) Determination of the release of Ag^+ from the hydrogels by treating with different concentrations of PBS for different periods of time by ICP-OES.

of Ag^+ demonstrated a positive correlation with time, achieving its maximum release after six hours. The reduced release of Ag^+ ions at a concentration of 0.01 M PBS significantly mitigated the accumulation of heavy metals. In contrast, the control group exhibited the highest Ag^+ release, likely attributable to the swelling of the mineralized hydrogel, as depicted in Figure 5(c). These findings suggest that the hydrogel synthesized *via* the bionano-mineralization method facilitates phosphate-responsive degradation and the subsequent release of encapsulated nanoparticles.

3.2.2. The antimicrobial properties of PAA-CaP@AgNps@exo hydrogel in vitro

The ring-of-inhibition assay compared the antimicrobial activities of AgNps, PAA-CaPs@AgNps, and PAA-CaPs@AgNps@exo hydrogels. The results indicated that the average diameters of the inhibitory rings for these three were 12, 15, and 23 mm for *S. aureus*, and 6, 7, and 11 mm for *E. coli* respectively, as shown in Figures. 6(a) and 6(b). These results showed that PAA-CaPs@AgNps@exo hydrogel was significantly more effective than the other two in inhibiting *E. coli* and *S. aureus*. The antimicrobial effect of PAA-CaPs@AgNps@exo hydrogel was further quantitatively evaluated by plate counting method, and the results showed that the inhibitory effect of the PAA-CaPs@AgNps@exo hydrogel was 100% against both *E. coli* and *S. aureus*, respectively (Figure 6c,d). It showed that the PAA-CaPs@AgNps@exo hydrogel had good bactericidal ability *in vitro*.

3.2.3. PAA-CaP@AgNps@exo hydrogel accelerates diabetic wound healing

To test whether the PAA-CaP@AgNps@exo hydrogel could accelerate diabetic wound healing, a rat model of diabetic wounds was established as shown in Figure 7(a). Wound images were captured on days 0, 4, 8, 12, and 16, as illustrated in Figure 7(b). The residual wound area was subsequently calculated for all groups at different time points. The results of the study showed that PAA-CaP@AgNps@exo hydrogel demonstrated a significantly faster wound healing rate than any of the other groups (Figure 7c). The dynamic recovery process of wound healing across different groups is shown in Figure 7(d). Skin tissue samples surrounding the wounds were subjected to HE and Masson staining. The results indicated complete epithelial formation in the PAA-CaP@AgNps@exo group. In addition, there was a substantial

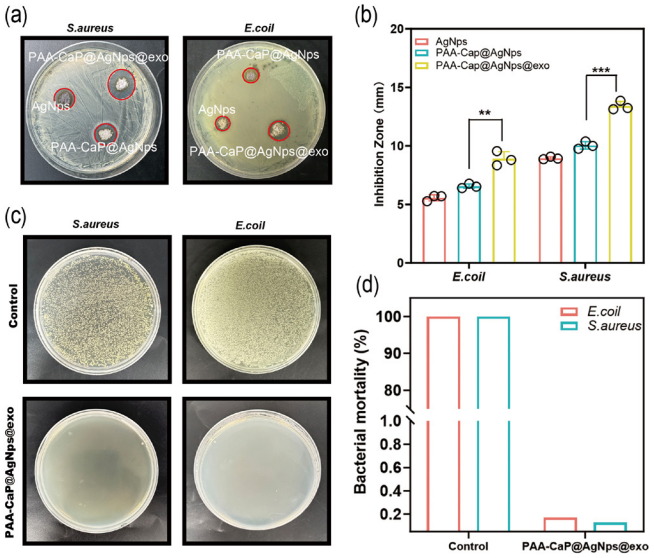

Figure 6. The antimicrobial properties of hydrogels *in vitro*. (a) Detection of the antimicrobial activities of silver nanoparticles (AgNps), PAA-CaPs@AgNps, and PAA-CaPs@AgNps@exo hydrogels on *S. aureus* and *E. coli* by the ring-of-inhibition assay; (b) Statistical results of the inhibitory rings of the AgNps, PAA-CaPs@AgNps, and PAA-CaPs@AgNps@exo hydrogels on *S. Aureus* and *E. coli*; (c) The antimicrobial effect of PAA-CaPs@AgNps@exo hydrogel evaluated by plate counting method; (d) Quantitative results of the inhibitory effect of PAA-CaPs@AgNps@exo hydrogel on *E. coli* and *S. Aureus* (n = 3, mean ± standard deviation (SD), *p < 0.05, **p < 0.01, ***p < 0.001). The black circles represent the experimental results from independent repetitions of the experiment.

migration of fibroblasts, a significant increase in blood vessel formation, and a significantly higher incidence of hair follicle formation than in the other groups (Figure 7e). According to these results, PAA-CaP@AgNps@exo hydrogel accelerates diabetic wound healing.

3.2.3. PAA-CaP@AgNps@exo hydrogel promotes angiogenesis, cell proliferation, anti-inflammation, re-epithelialization, and collagen deposition

To elucidate the mechanism of action of the PAA-CaP@AgNps@exo hydrogel in promoting wound healing, immunohistochemistry was employed to assess the expression of CD31, Ki67, and CD206 in the wound skin tissues of each group on day 8. The findings indicated that CD31 enhances neovascularization and increases the number of microvessels, thereby improving the nutritional and oxygen supply to the wound site, which is crucial for wound healing. In addition, Ki67 was significantly upregulated during the wound-healing process, playing a pivotal role in promoting cellular proliferation. $CD206^{+}$ M2-type macrophages inhibited wound inflammation and played a crucial role in tissue repair and regeneration [23]. Based on the results of this study, CD31, Ki-67, and CD206 expression levels in the wound tissue cells of diabetic rats treated with PAA-CaP@AgNps@exo hydrogel were significantly higher than those in other treatment groups (Figure 8a). According to these results, PAA-CaP@AgNps@exo hydrogel may speed the healing of diabetic wounds by promoting angiogenesis and promoting tissue regeneration.

CK10 is integral to the regeneration and repair processes of the epidermal layer of the skin. Furthermore, the differential expression of CK10 across various treatment groups at day 16 was observed to determine the extent of reepithelialization and epithelial differentiation. The results indicated that the PAA-CaP@AgNps@exo hydrogel-treated group exhibited higher CK10 expression and demonstrated a comparatively more mature epithelial structure than the other groups (Figure 8b). The principal collagen types present in the skin are type I collagen (COL I) and type III collagen (COL III). The appropriate deposition of these collagen types can enhance the strength of the skin, facilitate the healing process, and reduce the formation of scars.[24] In this study, the content of these two types of collagen in skin tissue on day 16 of wound healing was investigated using immunohistochemistry. The findings revealed that the group treated with PAA-CaP@AgNps@exo hydrogel exhibited higher COL I and COL III levels than any other group. As a result of these findings, PAA-CaP@AgNps@exo hydrogel is capable of remodeling the extracellular matrix effectively (Figure 8b). These findings indicate that the PAA-CaP@AgNps@exo hydrogel has the potential to expedite the healing of diabetic wounds by enhancing angiogenesis, cell proliferation, anti-inflammatory responses, re-epithelialization, and collagen deposition.

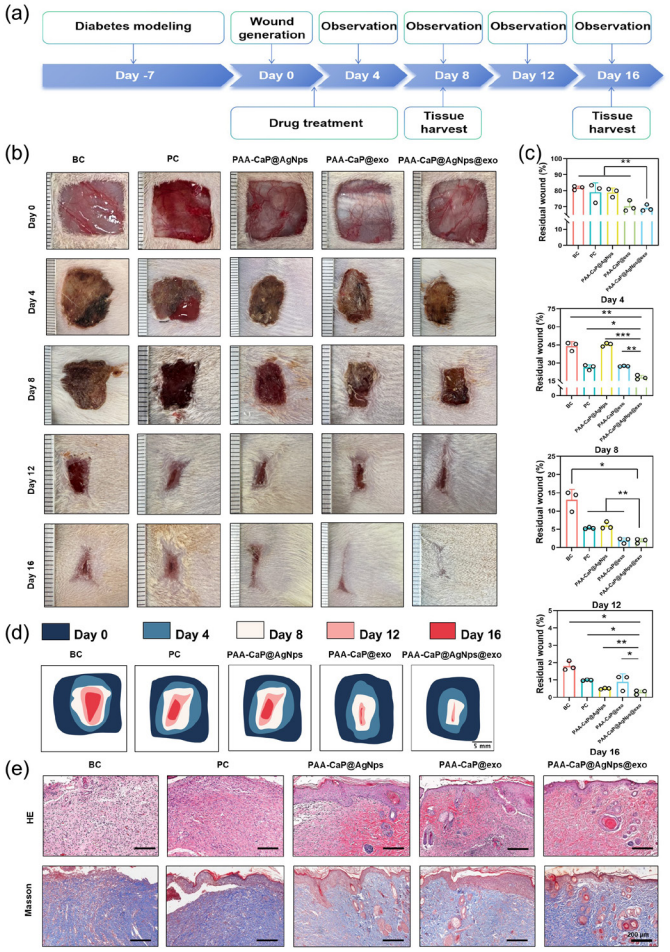

Figure 7. The antimicrobial properties of hydrogels *in vitro*. (a) Detection of the antimicrobial activities of AgNps, PAA-CaPs@AgNps, and PAA-CaPs@AgNps@exo hydrogels on *S. aureus* and *E. coli* by the ring-of-inhibition assay; (b) Statistical results of the inhibitory rings of the AgNps, PAA-CaPs@AgNps, and PAA-CaPs@AgNps@exo hydrogels on *S. Aureus* and *E. coli*; (c) The antimicrobial effect of PAA-CaPs@AgNps@exo hydrogel evaluated by plate counting method; (d) Quantitative results of the inhibitory effect of PAA-CaPs@AgNps@exo hydrogel on *E. coli* and *S. Aureus*. (n = 3, mean ± SD, *p < 0.05, **p < 0.01, ***p < 0.001). (e) Histological examination the skin tissue of different groups by Hematoxylin and eosin (HE) staining and Masson's trichrome (Masson) staining (50x). BC: Blank control, PC: Positive control.

3.2.4. PAA-CaP@AgNps@exo hydrogel accelerates bacteria-infected diabetic wound healing

Wound infection is a serious complication in diabetic wounds, significantly impacting the healing process. The predominant bacterial strains found in infected wounds are *S. aureus* and *E. coli*. This study aimed to assess the efficacy of PAA-CaP@AgNps@exo hydrogel in promoting healing in diabetic wounds infected with these bacteria. Surgically created wounds were infected with 1 x 10^{8} cells of *S. aureus* and *E. coli* in a 1:1 ratio. On the fourth day, the wounds were cleaned and treated with hydrogels. The established bacteria-infected diabetic wounds rat model is shown in Figure 9(a). The application of PAA-CaP@AgNps@exo hydrogel in treated wounds resulted in significant prevention of infection compared to non-treated infected wounds (Figure 9b,c). Histopathological analysis utilizing HE staining demonstrated enhanced fibroblast proliferation and granulation tissue

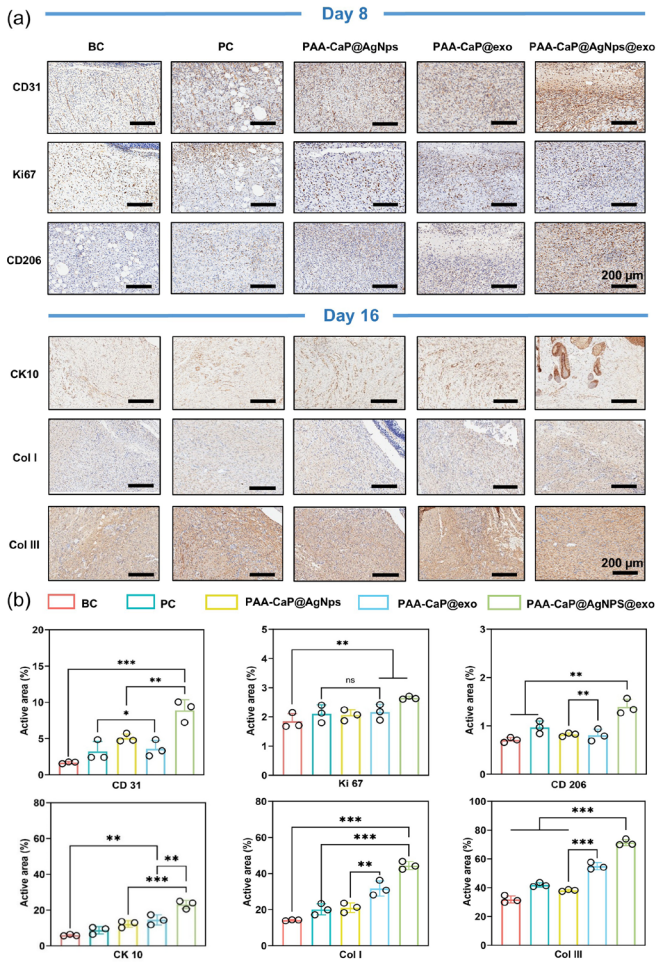

Figure 8. PAA-CaP@AgNps@exo hydrogel promotes angiogenesis, cell proliferation, anti-inflammation, re-epithelialization, and collagen deposition. (a) Immunohistochemical staining images of CD31, Ki67, CD206 expression on day 8, and CK10, COLI, COLIII expression on day 16 in the skin wounds of diabetes rats with different treatments; (b) The quantitative results of the CD31, Ki67, CD206, CK10, COLI, and COLIII expression detected by immuno- histochemical staining (n = 3, mean ± SD, *p < 0.05, **p < 0.01, ***p < 0.001). BC: Blank control, PC: Positive control, CD31: Platelet endothelial cell adhesion molecule-1, KI67: Marker of Proliferation Ki-67, CD206: Mannose Receptor C-Type 1, CK10: Cytokeratin 10, Col I: Collagen Type I, Col III: Collagen Type III. The black circles represent the experimental results from independent repetitions of the experiment.

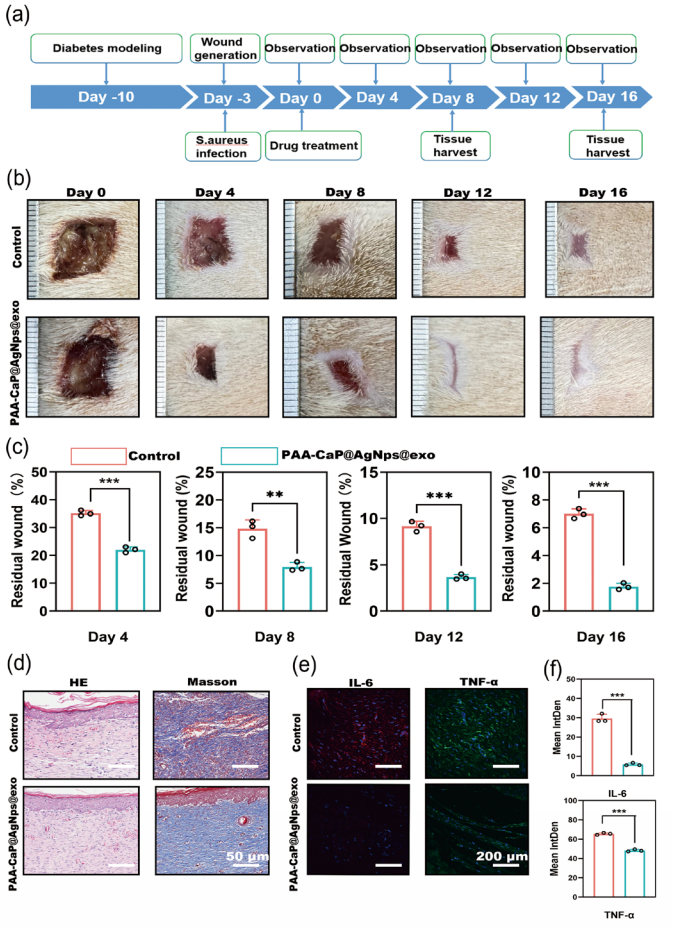

Figure 9. PAA-CaP@AgNps@exo hydrogel accelerates bacteria-infected diabetic wound healing. (a) Schematic diagram of the experimental procedure; (b) Images of wound healing of diabetic rats treated by PAA-CaP@AgNps@exo hydrogel at different time points; (c) Graph of statistical calculations of the residual wound area at different time points (n = 3, mean ± SD, *p < 0.05, **p < 0.01, ***p < 0.001); The black circles represent the experimental results from independent repetitions of the experiment. (d) Hematoxylin and eosin (HE) and Masson staining images of the skin wounds tissue on day 16; (e) Immunofluorescence staining images of Interleukin-6 (IL-6), and Tumor Necrosis Factor alpha (TNF-alpha), expression at the wound site on day 8; (f) Quantitative results of IL-1, and TNF-, expression in the regenerated skin tissue at day 8 (n = 3, mean ± SD, **p < 0.01, ***p < 0.001). (Hematoxylin and Eosin staining (HE) magnification 50x)

formation in wounds treated with PAA-CaP@AgNps@exo hydrogels. In addition, the treated wounds exhibited increased collagen deposition, as evidenced by Masson's trichrome staining, and were characterized by the presence of mature epithelial structures (Figure 9d). The inflammatory cytokines IL-1β and TNF-α at the wound site on day 8 of wound healing were detected using immunofluorescence. It revealed that PAA-CaP@AgNps@exo hydrogel effectively suppressed the presence of inflammatory cytokines IL-1β and TNF-α at the wound site, and it also effectively suppressed the release of inflammatory factors (Figure 9e,f). These results suggest the potential of PAA-CaP@AgNps@exo hydrogel in promoting accelerated healing in infected diabetic wounds.

3.3 Discussion

Diabetic wounds are particularly vulnerable to hyperglycemic conditions, which compromise the viability and functionality of skin cells, thereby impeding their proliferation and migration. This also results in reduced angiogenesis, collectively contributing to delayed wound repair [25]. Furthermore, the presence of elevated glucose levels serves as a nutrient source for bacteria, facilitating biofilm formation and subsequently leading to infections that further hinder the wound healing process [26]. Consequently, it is important to develop effective strategies to expedite wound healing in diabetic patients.

Over the past few years, researchers have been exploring the ability of exosomes derived from various cellular sources to facilitate the healing of challenging skin wounds [27]. It has been demonstrated that exosomes can facilitate the healing of wounds through their ability to regulate inflammatory responses, promote cell proliferation, promote migration, enhance angiogenesis, and inhibit scar formation [28-30]. These findings offer novel insights and strategies for the clinical management of diabetic wounds. UCB is easily collected and is frequently regarded as medical waste. Cord blood plasma contains a variety of biological substances, including proteins, enzymes, and active molecules secreted by cells. The isolation and purification of exosomes from human cord blood plasma results in the production of a substance that contains a multitude of biologically active elements with minimal immunogenicity. This has the potential to be utilized in the treatment of a variety of diseases [31,32]. Currently, little research has been conducted on the potential of UCB exosomes for the healing of diabetic wounds. Moreover, the precise mechanism of action remains uncertain. In this study, cord blood exosomes were initially obtained by centrifugation and were observed to repair the dysfunction of keratinocytes and HUVECs in high-glucose environments. Furthermore, the exosomes were found to increase the proliferation, migration, and tube-forming

ability of HUVECs. Sequencing analyses demonstrated that exosomes can influence cell function under high glucose conditions by modulating multiple signaling pathways, including the cell cycle. However, the direct use of exosomes for wound healing therapy has the problems of uncontrolled dosing and short half-life. In recent years, researchers have been practicing to develop effective biocompatible scaffolds as slow-release carriers for exosomes, and one of the more widely used carriers is hydrogel, which has good hydrophilicity, biocompatibility, and porous structure, and it can be effectively loaded with drugs or biologically active substances as a smart delivery system for wounds [33]. Bioprinting techniques for hydrogels also have a prospect in wound healing [34]. Studies have shown that exosomes can be combined with various forms of hydrogels, such as chitosan-silk hydrogel [35], nanofiber hydrogel [36], and natural methylcellulose-chitosan hydrogel [37], all of which have good mechanical properties, water retention, and cytocompatibility, and it can play a more stable and efficient role in the healing effect of exosomes on wounds.

This study draws inspiration from the mineralization of collagen fibers in living organisms. It demonstrates that PAA or other polyelectrolytes can self-assemble with biometallic ions such as Ca^{2+}, Cu^{2+}, and Zn^{2+} to form bionanomimetic mineralized hydrogels [38,39]. These hydrogels exhibit commendable biocompatibility and biodegradability. Furthermore, metal ions present in hydrogel matrices can interact with protein-based pharmaceuticals, forming aggregates that enhance drug loading while preserving long-term drug efficacy *in vivo* [40]. Conversely, biomineralized hydrogels can be readily modified by the surrounding reaction environment, enabling ion-responsive degradation and drug release. In the present study, a PAA-CaPs@AgNps@exo nanocomposite hydrogel was synthesized through the use of a PAA self-assembly procedure in conjunction with Ca^{2+} within a phosphate buffer. This process necessitated the utilization of PAA, possessing a carboxyl group (-COOH), as an inherent template. This template subsequently interacted with diffused Ca^{2+} and PO_4^{3-}, leading to the *in situ* encapsulation of Ag_3PO_4 nanoparticles and exosomes. The hydrogel can be utilized for the gradual release of exosomes in a solution of physiologically conditioned phosphate. The utilization of this hydrogel in the treatment of diabetic wounds has been demonstrated to facilitate the repair of the skin through the promotion of cell proliferation, collagen deposition, and neovascularization. The utilization of this hydrogel in bacterial-infected diabetic wounds has been demonstrated to exert antimicrobial effects as well as lower inflammatory factors. During this study, a biomimetically mineralized composite hydrogel was utilized to enable the controlled release of exosomes and nanosilver particles within the gel under physiological phosphate conditions. These results indicate that this approach enhanced wound healing through a variety of mechanisms, offering an innovative approach to diabetic wound dressings.

4. Conclusions

In this study, exosomes from UCB were isolated, characterized, and identified using a range of techniques, and subsequently assessed their wound-healing potential. The study findings revealed that these exosomes significantly enhanced the proliferation, migration, and angiogenesis of HUVECs under high-glucose conditions *in vitro*. Furthermore, the UCB-exo was loaded into the hydrogel along with AgNPs to fabricate a novel PAA-CaP@AgNps@exo hydrogel which showed bioactive multifunctional properties (accelerated the wound healing process) including phosphate-responsive release and antibacterial activity. Moreover, *in vivo* studies demonstrated that this hydrogel enhanced proliferation, collagen accumulation, angiogenesis, and prevention of infection within the wound site, thus accelerating the diabetic wound healing process. Therefore, the developed PAA-CaP@AgNps@exo hydrogels represent a highly promising therapeutic option for diabetic wound healing.

CRediT authorship contribution statement

Qianying Su: Conceptualization, investigation, data curation, and funding acquisition. **Peng Tuo and Huajian Li:** Data curation and methodology. **Hanyi Mei and Yahong Yuan:** Resources. **Abid Naeem:** Investigation and writing-review and editing. **Xiaoli Wang:** Conceptualization, supervision, funding acquisition, and writing-review and editing. All authors read and approved the final version of the manuscript.

Declaration of competing interest

All the authors declare no conflict of interests.

Declaration of Generative AI and AI-assisted technologies in the writing process

The authors confirm that there was no use of AI-assisted technology for assisting in the writing of the manuscript and no images were manipulated using AI.

Funding

This study was financially supported by the Advantages Discipline Group Medicine Project in Higher Education of Hubei Province (2024XKQY52), the Innovative Research Program for Undergraduates of Hubei Province (S202313249002).

Acknowledgments

The authors thank the Institute of Biomedical Research Center of the Hubei University of Medicine for providing instrumental and equipment support. We thank Professor Weikang Hu, School of Materials Science and Engineering, Hubei University, for his help and valuable suggestions.

References

1. Schaper, N., van Netten, J., Apelqvist, J., Bus, S., Hinchliffe, R., Lipsky, B., 2020. Practical Guidelines on the prevention and management of diabetic foot disease (IWGDF 2019 update). *Diabetes/Metabolism Research and Reviews* **36 Suppl 1**, e3266. doi: https://doi.org/10.1002/dmrr.3266
2. Bowers, S., Franco, E., 2020. Chronic wounds: Evaluation and management. *American Family Physician* **101**, 159-166.
3. Oyebode, O., Jere, S., Houreld, N., 2023. Current therapeutic modalities for the management of chronic diabetic wounds of the foot. *Journal of Diabetes Research* **2023**, 1359537. doi: https://doi.org/10.1155/2023/1359537
4. Bian, D., Wu, Y., Song, G., Azizi, R., Zamani, A., 2022. The application of mesenchymal stromal cells (MSCs) and their derivative exosome in skin wound healing: A comprehensive review. *Current Stem Cell Research & Therapy* **13**, 24. doi: https://doi.org/10.1186/s13287-021-02697-9
5. Long, R., Wang, S., 2024. Exosomes from preconditioned mesenchymal stem cells: Tissue repair and regeneration. *Regeneration Therapy* **25**, 355-366. doi: 10.1016/j.reth.2024.01.009
6. Zhou, C., Zhang, B., Yang, Y., Jiang, Q., Li, T., Gong, J., Tang, H., Zhang, Q., 2023. Stem cell-derived exosomes: Emerging therapeutic opportunities for wound healing. *Stem Cell Research Therapy* **14**, 107. doi: https://doi.org/10.1186/s13287-023-03345-0
7. Zhang, A., Liu, Y., Qin, D., Sun, M., Wang, T., Chen, X., 2020. Research status of self-healing hydrogel for wound management: A review. *International Journal of Biological Macromolecules* **164**, 2108-2123. doi: 10.1016/j.ijbiomac.2020.08.109
8. Hu, W., Wang, W., Chen, Z., Chen, Y., Wang, Z., 2024. Engineered exosomes and composite biomaterials for tissue regeneration. *Theranostics* **14**, 2099-2126. doi: 10.7150/thno.93088
9. Wang, P., Theocharidis, G., Vlachos, I., Kounas, K., Lobao, A., Shu, B., Wu, B., Xie, J., Hu, Z., Qi, S., Tang, B., Zhu, J., Veves, A., 2022. Exosomes derived from epidermal stem cells improve diabetic wound healing. *Journal of Investigative Dermatology* **142**, 2508-2517. doi: 10.1016/j.jid.2022.01.030
10. Yang, J., Chen, Z., Pan, D., Li, H., Shen, J., 2020. Umbilical cord-derived mesenchymal stem cell-derived exosomes combined pluronic f127 hydrogel promote chronic diabetic wound healing and complete skin regeneration. *International Journal of Nanomedicine* **15**, 5911-5926. doi: 10.2147/IJN.S249129
11. Yuan, M., Liu, K., Jiang, T., Li, S., Chen, J., Wu, Z., Li, W., Tan, R., Wei, W., Yang, X., Dai, H., Chen, Z., 2022. GelMA/PEGDA microneedles patch loaded with HUVECs-derived exosomes and Tazarotene promote diabetic wound healing. *Journal of Nanobiotechnology* 20, 147. doi: https://doi.org/10.1186/s12951-022-01354-4
12. Rahim, K., Saleha, S., Zhu, X., Huo, L., Basit, A., Franco, O., 2017. Bacterial contribution in chronicity of wounds. *Microbial Ecology* **73**, 710-721. doi: 10.1007/s00248-016-0867-9
13. Spirescu, V., Chircov, C., Grumezescu, A., Vasile, BŞ., Andronescu, E., 2021. Inorganic nanoparticles and composite films for antimicrobial therapies.

International Journal of Molecular Sciences **22**, 4595. doi: https://doi.org/10.3390/ijms22094595
14. Hashem, A., Shehabeldine, A., Ali, O., Salem, S., 2022. Synthesis of chitosan-based gold nanoparticles: antimicrobial and wound-healing activities. *Polymers (Basel)* **14**, 2293. doi: https://doi.org/10.3390/polym14112293
15. Li, J., Liu, X., Tan, L., Cui, Z., Yang, X., Liang, Y., Li, Z., Zhu, S., Zheng, Y., Yeung, K., Wang, X., Wu, S., 2019. Zinc-doped Prussian blue enhances photothermal clearance of Staphylococcus aureus and promotes tissue repair in infected wounds. *National Communication* **10**, 4490. doi: https://doi.org/10.1038/s41467-019-12429-6
16. Pangprasit, N., Thammawong, Y., Kulsirorat, A., Chuammitri, P., Kongkaew, A., Intanon, M., Suriyasathaporn, W., Pikulkaew, S., Chaisri, W., 2023. Titanium dioxide nano-formulation: characterization, antimicrobial activity, and wound healing in animals. *Animals (Basel)* **13**, 2688. doi: https://doi.org/10.3390/ani13172688
17. Sandoval, C., Ríos, G., Sepúlveda, N., Salvo, J., Souza-Mello, V., Farías, J., 2022. Effectiveness of copper nanoparticles in wound healing process using in vivo and in vitro studies: A systematic review. *Pharmaceutics* **14**, 1838. doi: https://doi.org/10.3390/pharmaceutics14091838
18. Xu, L., Wang, Y., Huang, J., Chen, C., Wang, Z., Xie, H., 2020. Silver nanoparticles: Synthesis, medical applications and biosafety. *Theranostics* **10**, 8996-9031. doi: 10.7150/thno.45413
19. Tang, S., Zheng, J., 2018. Antibacterial activity of silver nanoparticles: Structural effects. *Advanced Healthcare Materials* **7**, e1701503. doi: https://doi.org/10.1002/adhm.201701503
21. Nikravesh, N., Davies, O., Azoidis, I., Moakes, R., Marani, L., Turner, M., Kearney, C., Eisenstein, N., Grover, L., Cox, S., 2019. Physical structuring of injectable polymeric systems to controllably deliver nanosized extracellular vesicles. *Advanced Healthcare Materials* **8**, e1801604. doi: https://doi.org/10.1002/adhm.201801604
20. Hu, W., Chen, Z., Chen, X., Feng, K., Hu, T., Huang, B., Tang, J., Wang, G., Liu, S., Yang, G., Wang, Z., 2023. Double-network cellulose-based hybrid hydrogels with favourable biocompatibility and antibacterial activity for wound healing. *Carbohydrate Polymers* **319**, 121193. doi: https://doi.org/10.1016/j.carbpol.2023.121193
22. Velnar, T., Gradisnik, L., 2018. Tissue augmentation in wound healing: The role of endothelial and epithelial cells. *Medical Archives* **72**, 444-448. doi: 10.5455/medarh.2018.72.444-448
23. Ogle, M., Krieger, J., Tellier, L., McFaline-Figueroa, J., Temenoff, J., Botchwey, E., 2018. Dual affinity heparin-based hydrogels achieve pro-regenerative immunomodulation and microvascular remodeling. *ACS Biomaterials Science & Engineering* **4**, 1241-1250. doi: 10.1021/acsbiomaterials.6b00706
24. Wilkinson, H., Hardman, M., 2020. Wound healing: Cellular mechanisms and pathological outcomes. *Open Biology* **10**, 200223. doi: https://doi.org/10.1098/rsob.200223
25. Patel, S., Srivastava, S., Singh, M., Singh, D., 2019. Mechanistic insight into diabetic wounds: Pathogenesis, molecular targets and treatment strategies to pace wound healing. *Biomedicine & Pharmacotherapy* **112**, 108615. doi: https://doi.org/10.1016/j.biopha.2019.108615
26. Ghotaslou, R., Memar, M., Alizadeh, N., 2018. Classification, microbiology and treatment of diabetic foot infections. *Journal of Wound Care* **27**, 434-441. doi: 10.12968/jowc.2018.27.7.434
27. Lv, H., Liu, H., Sun, T., Wang, H., Zhang, X., Xu, W., 2022. Exosome derived from stem cell: A promising therapeutics for wound healing. *Frontiers in Pharmacology* **13**, 957771. doi: https://doi.org/10.3389/fphar.2022.957771
28. He, L., Zhu, C., Jia, J., Hao, X., Yu, X., Liu, X., Shu, M., 2020. ADSC-Exos containing MALAT1 promotes wound healing by targeting miR-124 through activating Wnt/β-catenin pathway. *Bioscience reports* **40**, BSR20192549. doi: https://doi.org/10.1042/BSR20192549
29. Hu, Y., Tao, R., Chen, L., Xiong, Y., Xue, H., Hu, L., Yan, C., Xie, X., Lin, Z., Panayi, A., Mi, B., Liu, G., 2021. Exosomes derived from pioglitazone-pretreated MSCs accelerate diabetic wound healing through enhancing angiogenesis. *Journal of Nanobiotechnology* **19**, 150. doi: https://doi.org/10.1186/s12951-021-00894-5
30. Yan, C., Chen, J., Wang, C., Yuan, M., Kang, Y., Wu, Z., Li, W., Zhang, G., Machens, H., Rinkevich, Y., Chen, Z., Yang, X., Xu, X., 2022. Milk exosomes-mediated miR-31-5p delivery accelerates diabetic wound healing through promoting angiogenesis. *Drug Delivery* **29**, 214-228. doi: 10.1080/10717544.2021.2023699
31. Hu, Y., Rao, S., Wang, Z., Cao, J., Tan, Y., Luo, J., Li, H., Zhang, W., Chen, C., Xie, H., 2018. Exosomes from human umbilical cord blood accelerate cutaneous wound healing through miR-21-3p-mediated promotion of angiogenesis and fibroblast function. *Theranostics* **8**, 169-184. doi: 10.7150/thno.21234
32. Liu, J., Sun, W., Liu, C., Na, Q., 2023. umbilical cord blood-derived exosomes in maternal-fetal disease: A review. *Reproductive Sciences* **30**, 54-61. doi: 10.1007/s43032-022-00879-1
33. Qi, L., Zhang, C., Wang, B., Yin, J., Yan, S., 2022. Progress in hydrogels for skin wound repair. *Macromolecular Bioscience* **22**, e2100475. doi: https://doi.org/10.1002/mabi.202100475
34. Wang, Z., Liang, X., Wang, G., Wang, X., Chen, Y., 2023. Emerging bioprinting for wound healing. *Advanced Materials* e2304738. doi: https://doi.org/10.1002/adma.202304738
35. Shi, Q., Qian, Z., Liu, D., Sun, J., Wang, X., Liu, H., Xu, J., Guo, X., 2017. GMSC-derived exosomes combined with a chitosan/silk hydrogel sponge accelerates wound healing in a diabetic rat skin defect model. *Frontiers in Physiology* **8**, 904. doi: https://doi.org/10.3389/fphys.2017.00904
36. Han, S., Yang, H., Ni, X., Deng, Y., Li, Z., Xing, X., Du, M., 2023. Programmed release of vascular endothelial growth factor and exosome from injectable chitosan nanofibrous microsphere-based PLGA-PEG-PLGA hydrogel for enhanced bone regeneration. *International Journal of Biological Macromolecules* **253**, 126721. doi: https://doi.org/10.1016/j.ijbiomac.2023.126721
37. Wang, C., Liang, C., Wang, R., Yao, X., Guo, P., Yuan, W., Liu, Y., Song, Y., Li, Z., Xie, X., 2019. The fabrication of a highly efficient self-healing hydrogel from natural biopolymers loaded with exosomes for the synergistic promotion of severe wound healing. *Biomaterials Science* **8**, 313-324. doi: 10.1039/c9bm01207a
38. Sun, S., Mao, L., Lei, Z., Yu, S., Cölfen, H., 2016. Hydrogels from amorphous calcium carbonate and polyacrylic acid: Bio-inspired materials for "mineral plastics". *Angewandte Chemie (International ed. in English)* **55**, 11765-9. doi: 10.1002/anie.201602849
39. Xie, C., Lu, X., Han, L., Xu, J., Wang, Z., Jiang, L., Wang, K., Zhang, H., Ren, F., Tang, Y., 2016. Biomimetic mineralized hierarchical graphene oxide/chitosan scaffolds with adsorbability for immobilization of nanoparticles for biomedical applications. *ACS Applied Materials & Interfaces* **8**, 1707-17. doi: 10.1021/acsami.5b09232
40. Lao, A., Wu, J., Li, D., Shen, A., Li, Y., Zhuang, Y., Lin, K., Wu, J., Liu, J., 2023. Functionalized metal-organic framework-modified hydrogel that breaks the vicious cycle of inflammation and ROS for repairing of diabetic bone defects. *Small* **19**, e2206919. doi: https://doi.org/10.1002/smll.202206919